Interception of a Projectile Using a Human Vision-Based Strategy

Justin A. Borgstadt and Nicola J. Ferrier*
Department of Mechanical Engineering
University of Wisconsin-Madison
justin@mechatron.me.wisc.edu ferrier@mechatron.me.wisc.edu

Abstract

Visual-servoing tasks for mobile robots characteristically require the processing of vast amounts of navigational information which can impede the performance of even the most well designed systems. This paper investigates the idea of using a simple human-based strategy to accomplish the task of using a mobile robot to intercept a projectile. This vision based control strategy relies on a *single* image-based parameter whose sign corresponds to a decision whether to run forward or backward for successful interception. Assuming the ball can be tracked easily in real time by the mobile robot's vision system, computational time for motion decision making and control is minimized. We examine and develop several motion control strategies which incorporate the robot's velocity and acceleration in addition to this human-based strategy. The simplest of these strategies is used with a mobile robot and demonstrates results similar to a human both in simulation and real-world application.

Keywords: *image-based visual servo, robot games*

1 Introduction

Much effort has been given to the design of robust robotic systems which can perform complicated tasks quickly and efficiently. One method of design involves extensive 3-D dynamic modeling of both the workspace and robot. While this approach has been proven to be effective in real-time for even difficult tasks [1] the cost in terms of required hardware, computational power, and design time can be extensive.

McLeod and Dienes present an empirical model based on how humans intercept balls projected towards them [3]. Their basic assumption is that the fielder cannot possibly know exactly where the ball will land by calculating velocity, projection angle, wind resistance, and other factors affecting the flight path in the time allowed. However, the human fielder does learn to catch the ball very effectively. Their goal was to discover the "unconscious" learned algorithm which allows the fielder to succeed. Their proposed model states that if a fielder runs "at a speed which keeps $d^2(\tan\alpha)/dt^2$ zero, where α is the vertical angle of gaze as they watch the ball" the fielder will arrive at the point where the ball will land at the exact same time the ball arrives [3]. Evidence for this model was gathered by videotaping several different human fielder's catching balls of varying projectile motions. They suggest that the sign of $d^2(\tan\alpha)/dt^2$ may be used as an input to a mechanism designed to catch a projectile telling it whether to move forward, backward, or stay stationary. They do not, however, discuss any possible algorithms that would determine other aspects of the motion (such as velocity, acceleration, etc).

The sign of $d^2(\tan\alpha)/dt^2$ may be able to tell the fielder which direction to move but several issues need to be addressed in a control structure, such as the determination of the fielder's velocity and acceleration. The first part of this paper describes the details of how the robotic fielder tracks the ball and calculates the motion parameter $d^2(\tan\alpha)/dt^2$. Then four different motion control strategies are investigated through simulations to determine which strategy best utilizes the sign of $d^2(\tan\alpha)/dt^2$ to allow a robotic fielder to successfully intercept projected balls. The last part of this paper deals with applying a successful simulated motion control strategy to a real world situation. A ball is projected in real-time towards a mobile robot equipped with a vision system to demonstrate the feasibility of using the human-based model for visual-servoing.

2 Control Parameter

In order to accurately compute the motion parameter $d^2(\tan\alpha)/dt^2$ three things need to be achieved: image based tracking of the projectile, projectile fixation, and error minimization in the computation of

*Person to whom correspondence should be addressed. This research supported in part by NSF IRI-9703352.

the discrete variables $\tan\alpha$ and $d(\tan\alpha)/dt$ between successive frames. In this investigation a Real World Interface (RWI), Inc. B21 Mobile Robot is used with a head mounted DP pan-tilt unit and Sony CCD camera.

Images taken with the CCD camera are grey scaled images. Image based tracking of the projectile is achieved by using a white ball on a dark background and using a threshold value with the moment equations given by Corke [2] to determine the centroid of the ball. Since the ball is assumed to be traveling in a purely vertical direction with respect to the robot the computational time per frame is reduced by narrowing the window size of processed image data.

In order to fixate on the projectile and keep it in the field of view the tilt unit on the robot is used to help keep the projection of the centroid at the center of the image or along the camera frame z-axis (Figure 1). The tilt angle β_n is the angle required to bring the centroid of the projectile to the center of the image in the n^{th} frame. β_n is computed using the classical pinhole model and is given by:

$$\beta_n = \tan^{-1}\frac{0.5h - v}{f} \tag{1}$$

The gaze angle α_n for the n^{th} frame is then given by (Figure 1) $\alpha_n = \alpha_{n-1} + \beta_n$.

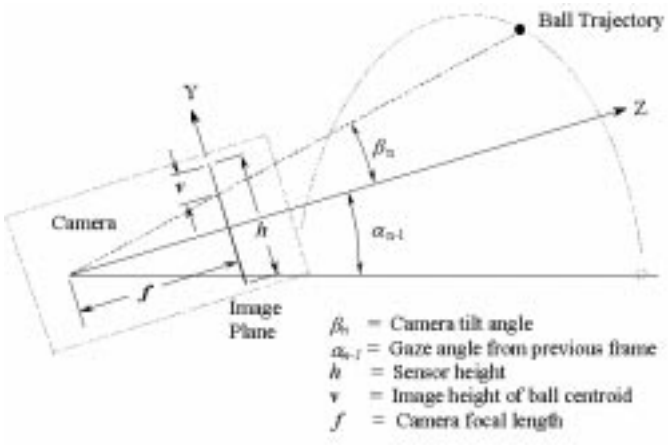

Figure 1: Geometry of Gaze Angle, α_n and Fixation Task

The tilt angle β_n is calculated independently for each frame and used as the input to tilt the camera and follow the ball for the entire motion. The gaze angle α_n , however, is incremented for each consecutive frame by β_n starting from the initial frame at $n = 1$ with tilt angle β_1 and $\alpha_0 = 0$.

With a minimum of three values for the gaze angle, α_n, α_{n-1}, and α_{n-2}, from three successive images and their corresponding tangent values, $\tan\alpha_n$, $\tan\alpha_{n-1}$, and $\tan\alpha_{n-2}$, the discrete motion parameter $d^2(\tan\alpha_n)/dt^2$ is computed by second difference methods [4].

Two factors contribute to errors in the calculation of $d^2(\tan\alpha_n)/dt^2$. First, $d^2(\tan\alpha_n)/dt^2$ is at best an an average value over a time period of $2dt$. Secondly, the robot frame of reference from which α_n is being measured is moving relative to the projectile at a variable rate. The higher the relative velocity between the robot and projectile the more error will be incurred in the successive values of α_n and, therefore, $d^2(\tan\alpha_n)/dt^2$. A way to decrease both effects is to decrease the value of dt. However, a limit exists due to the time required to process the image data and compute the centroid of the projectile in the image. For these tests a minimum value of $dt = 100ms$ is being used.

3 Motion Control Strategies

Human fielder studies suggest from that the sign of $d^2(\tan\alpha_n)/dt^2$ could be used as an input to tell the robotic fielder whether to run forward, run back, or remain stationary. If the sign of $d^2(\tan\alpha_n)/dt^2$ is negative this indicates the projectile is beginning to drop in front of the fielder and hence the fielder needs to run forward for a successful interception. For the case where the sign is positive the ball is beginning to pass overhead and the fielder needs to run backward. If the value of $d^2(\tan\alpha_n)/dt^2$ is zero then the fielder needs to remain stationary [3]. The simple control architecture implemented for the robotic fielder is shown in Figure 2 where the motion controller uses the sign of $d^2(\tan\alpha_n)/dt^2$ to help determine the fielder's next move. Although the sign of $d^2(\tan\alpha_n)/dt^2$ tells the fielder which direction to move, how does the fielder determine its velocity?

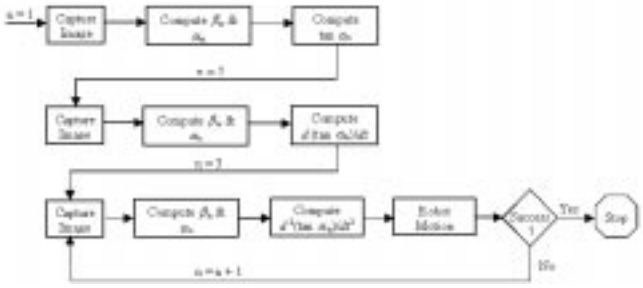

Figure 2: Robotic Fielder Control Architecture

In McLeod's and Dienes' first experiment the human fielder started 45m away from the projection point and four separate balls were launched each with

a projection angle of 45^o but with varying initial velocities. As can be seen in Figure 3 the four balls landed at varying distances to the fielder's initial position: -2.9m behind, +3.2m in front, +5.6m in front and +8.4m in front. This experiment was used to show how the value of $d^2(\tan\alpha_n)/dt^2$ and the fielder's velocity changes as the fielder runs to intercept balls with trajectories of varying length. Their second experiment is used to show that the fielder does not know where to go to successfully intercept the ball. This was done by launching one ball at a 45^o angle and a second ball at a 64^o angle as can be seen in Figure 3. The fielder started 45m away from the projection point and the initial velocities were adjusted to ensure that both balls landed exactly +8.5m in front of the fielder. These same ball trajectories are used in the simulation experiments presented in this paper.

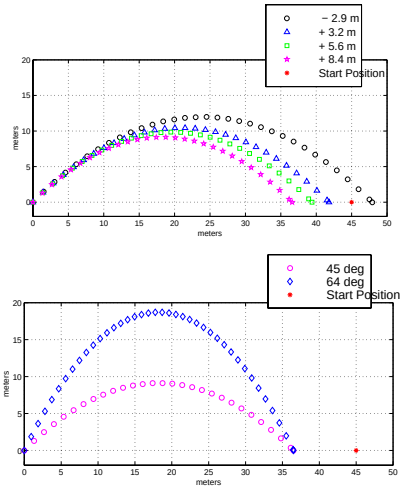

Figure 3: Ball Trajectories used. (a) Experiment 1: varying Length. (b) Experiment 2: Varying Initial Projection Angle

Several different motion control strategies were developed using Matlab simulations and tested under the conditions of both the first and second experiments presented by McLeod and Dienes. The most significant of these strategies are presented here in chronological order.

3.1 Motion Parameter Based Control

McLeod and Dienes suggest a relationship with the magnitude of $d^2(\tan\alpha)/dt^2$ where the fielder should run faster for relatively larger values and slower for relatively smaller values. One problem with this strategy occurs towards the end of the flight when the fielder is near the ball and the gaze angle, α_n, is approaching its maximum value. The relationship between α_n and $\tan\alpha_n$ is non-linear recalling that $\tan\alpha_n$ approaches infinity as α_n approaches 90^o.

Another problem results from the relative motion between the ball and the fielder. Small displacements in the fielder's position relative to the ball towards the end of the flight creates large changes in the value of α_n. Coupled with the increased sensitivity of $\tan\alpha_n$ to α_n at the end of the flight the resulting changes in magnitude of $d(\tan\alpha_n)/dt$ and $d^2(\tan\alpha_n)/dt^2$ are catastrophic. The simulated fielder moves faster and faster as he tries to position for a successful catch especially for balls with large initial projection angles. The result is instability and the fielder quickly moves away from the point of a successful interception. This indicates that a human fielder uses a visual cue other than or in addition to $d^2(\tan\alpha_n)/dt^2$.

3.2 Distance to Ball Strategy

Another strategy, the omniscient fielder, assumes that the fielder can judge the distance to the ball and thus would know exactly what distance to move in order to keep $d(\tan\alpha_n)/dt$ a constant (i.e. $d^2(\tan\alpha)/dt^2 = 0$). Using a simulation to generate the x and y coordinates of the ball and simulated fielder the exact distance, d_n, between the fielder and ball are known at each sample time as well as the value of α_n. This case is studied as it demonstrates the utility of the angular measurement in determining fielder motion.

The initial value of $d(\tan\alpha_2)/dt$ between the first $(n = 1)$ and second $(n = 2)$ frames is then used to predict the exact distance the fielder needs to move in order to keep $d(\tan\alpha_n)/dt$ a constant. For $n > 2$ this is done by first calculating at what gaze angle the ball should be in the fielder's view in order that,

$$\frac{d(\tan\alpha_n)}{dt} = \frac{d(\tan\alpha_2)}{dt} \tag{2}$$

This desired gaze angle, α_n^*, is given by,

$$\alpha_n^* = \tan^{-1}\left[\left(\frac{d(\tan\alpha_2)}{dt}\right) * dt \; + \; \tan\alpha_{n-1}\right] \tag{3}$$

From the values of the distance between the fielder and the ball and α_n the relative vertical distance, y_n, and horizontal distance, x_n, can be computed by,

$$y_n = d_n \sin\alpha_n, \quad x_n = d_n \cos\alpha_n \tag{4}$$

In order to make $\alpha_n \approx \alpha_n^*$ the robot fielder is moved a distance, δ_n, given by,

$$\delta_n = \frac{y_n}{(\tan\alpha_n^*)} - x_n \tag{5}$$

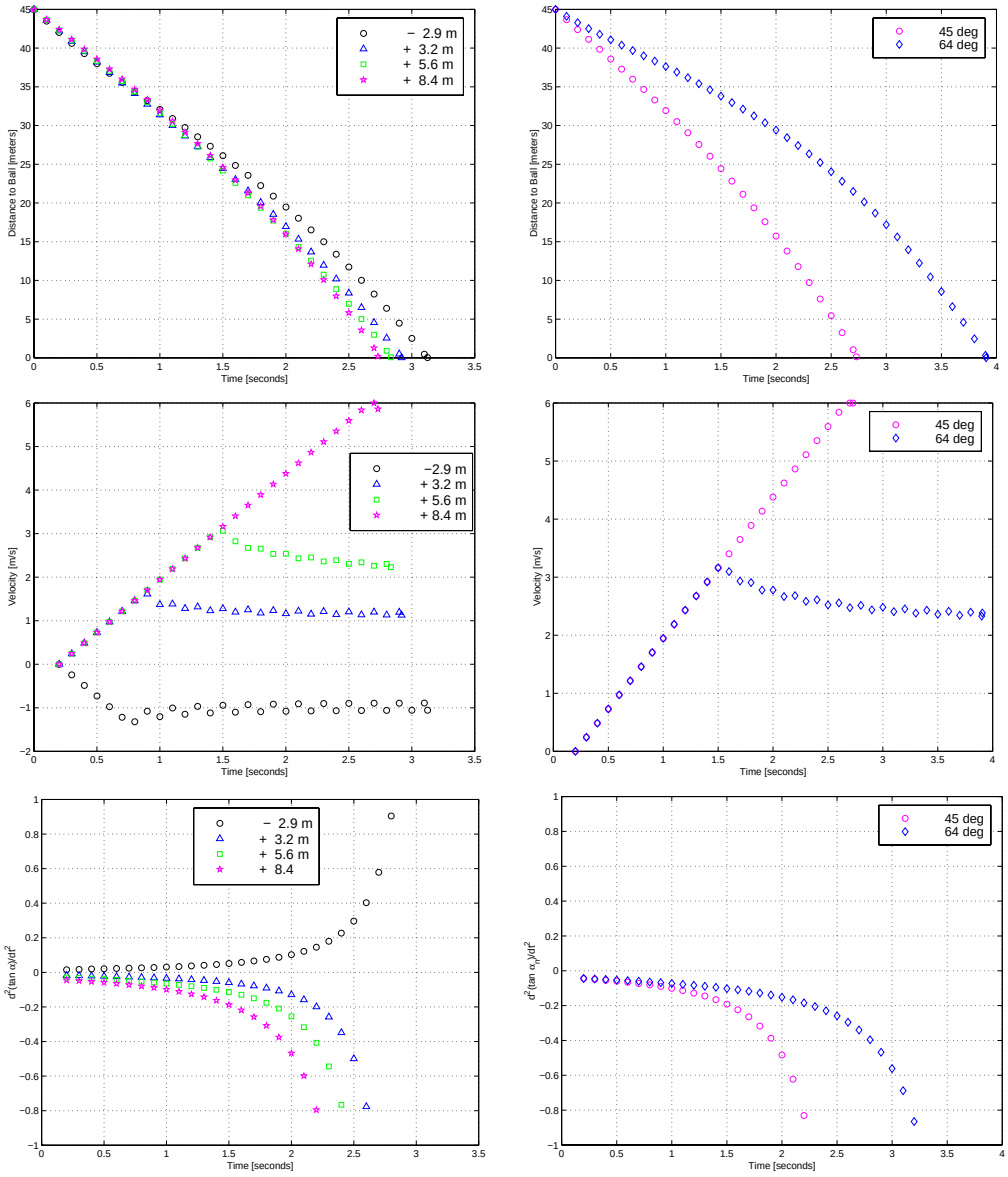

Simulation 1 Results

Simulation 2 Results

Figure 4: Simulation results for distance to ball strategy (column 1: simulation 1, column 2: simulation 2). Row 1: Distance between the fielder and ball vs. time, Row 2: Fielder velocity vs. time, and Row 3: $d^2(\tan\alpha_n)/dt^2$ vs. time.

The sign of δ_n corresponds to the sign of $d^2(\tan\alpha_n)/dt^2$ and is used with the value of dt to calculate the velocity of the simulated fielder between frames over the entire motion.

The first set of simulations test ball trajectories of varying length (Figure 3). Using the distance to ball strategy the relative distance between the fielder and ball for each of the four trajectories is shown in in Figure 4 (column 1). This strategy was successful. The fielder was able to intercept all four balls indicated by the relative distance, d_n, approaching zero for all four cases. In Figure 4(middle) the velocities for each of the four trajectories are plotted versus time. The fielder can be seen initially accelerating at his maximum rate for all four cases. For the +8.4 m case the fielder accelerates during the entire motion indicating this is as far as he can run in the time allowed. Figure 4(bottom) shows the value of $d^2(\tan\alpha)/dt^2$ for all four cases was relatively close to zero until the end of each flight. This drift is due to the lag by one frame of the calculation of δ_n and the fielder's subsequent motion. For the +3.2m, +5.6m, and +8.4m cases the

negative drift indicates the ball is dropping in front of the fielder while the positive drift for the -2.9m case indicates the ball is passing overhead.

The second set of simulations test (Figure 3 with ball trajectories of varying projection angle. As can be seen in Figure 4 (column 2) the fielder intercepts both balls as δ_n approaches zero for both cases. In Figure 4(middle) the fielder's velocities are plotted for both trajectories. For the ball with the 45^o projection angle the fielder must run (and accelerate) as fast as he can to successfully intercept the ball. For the ball with the 64^o projection angle the fielder accelerates at his maximum rate and then adjusts his velocity after 1.5 seconds and runs at an almost constant rate. McLeod and Dienes argue that if the human fielder knew where to go to successfully intercept the ball he would run at a maximum speed to the exact landing point and, if allowed enough time, wait there to make the interception. As indicated by the ball projected at $64^o$the simulated fielder does not stop but keeps running at an almost constant velocity. Therefore, the simulated fielder using the distance to ball strategy behaves in much the same way as the human fielder. As in experiment 1, the value of $d^2(\tan\alpha)/dt^2$ stays relatively close to zero with negative drift towards the end of the flight of both balls. This indicates again that the balls dropped in front of the simulated fielder at the end of each flight.

Figure 5 is also included to show the actual gaze angle, α_n, as seen by the simulated fielder and the desired gaze angle, α_n^*, at each sample time for the - 2.9m and +8.4m cases. Since the value of α_n^* is dependent on α_{n-1} the difference between the two angles is cumulative over the course of the motion. However, this does not seem to greatly affect the successfulness of this strategy.

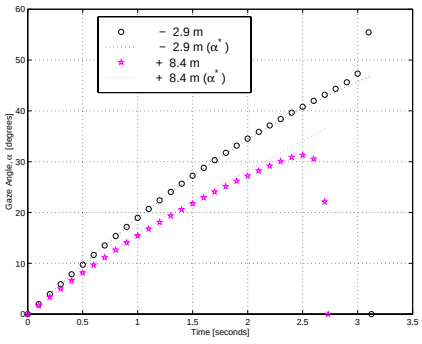

Figure 5: α_n and α_n^* vs. Time

While the distance to ball strategy is successful and appears to closely matches human studies, the goal of servoing based purely on image information is not accomplished. Calculating the distance between the fielder and the ball makes the fielder dependent on 3-D information. Although stereo imaging could provide 3-D information, the robot (and/or human) has a small baseline to which the stereo computation is notoriously sensitive. These are undesirable characteristics and probably unrealistic cues for successful human interception.

3.3 Time to Contact Strategy

Another strategy implements the value of the time to contact between the ball and the fielder calculated from the ball image height, l_n and its first derivative with respect to time, $d(l_n)/dt$. The time to contact, τ_n, is given by [5] ,

$$\tau_n = l_n \setminus \frac{d(l_n)}{dt} \tag{6}$$

This can be a useful parameter for many visual-servoing applications where only image information is available. However, this derivation assumes that the object in the image is traveling towards the camera in a straight line with constant velocity. In Figure 6 the value of the time to contact is computed for five different projectiles. The simulated fielder stays stationary 45m from the projection point and each ball is projected at 64^o. This initial velocity is adjusted in order that the balls will land +8.5m in front, +4.0m in front, at the fielder's position, -4.0m behind, and -8.5m behind the fielder.

Because the ball is not traveling in a straight line towards the fielder and does not have a constant velocity in the fielder's viewing frame the time to contact is not linear. The time to contact actually increases at the beginning of the flight for all five projectiles especially for the -8.5m behind projectile. If the fielder was allowed to move to intercept the ball the value of the time to contact was found to approach infinity at certain points in the flight because there was no relative change in the balls image height between frames ($d(l_n)/dt = 0$). This was especially true for relatively high projection angles.

Any attempt to use relative magnitudes of τ_n between successive frames as a means of velocity control for the fielder led to instabilities at points of infinite time to contact. Even by filtering these points out the fielder still did not converge on the ball using this strategy.

3.4 Constant Acceleration Strategy

The final control strategy developed sets the fielder's acceleration, a, to a constant value. The fielder then either increases or decreases velocity depending on the

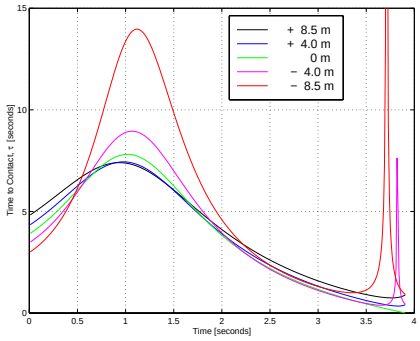

Figure 6: Time to Contact, τ_n vs. Time

sign of $d^2(\tan\alpha)/dt^2$ by a constant factor $a\,dt$. Using first principles the fielder can compute how fast he needs to run based purely on image information. The fielder's velocity, v_n, is given by,

$$v_n = v_{n-1} + m_n\, a\, dt \tag{7}$$

where

$$m_n = \begin{cases} 1 & \text{for } d^2(\tan\alpha_n)/dt^2 > 0 \\ -1 & \text{for } d^2(\tan\alpha_n)/dt^2 < 0 \\ 0 & \text{for } d^2(\tan\alpha_n)/dt^2 = 0 \end{cases} \tag{8}$$

Using simulations with ball trajectories of varying length (Figure 3) this strategy is shown in Figure 7 (column 1) to be successful. The distance, d_n, between the fielder and the ball approaches zero at the end of the flight for each trajectory.

In Figure 7(middle) the velocities for each case appear more erratic than for the distance to ball strategy given in Section 3.2. However, this appears to correspond to the more erratic velocities recorded for human fielders [3]. Figure 7(bottom row) shows the value of $d^2(\tan\alpha_n)/dt^2$ for all four cases stays closer to zero longer than the values recorded using the distance to ball strategy in Section 3.2 (Figure 4(bottom row)). However, there are substantial deviations towards the end of each flight. This is due to the inherent error caused by the control strategy itself. For the +8.4m flight the ball drops in front of the simulated fielder as indicated by the drop in $d^2(\tan\alpha_n)/dt^2$ at the end of the flight. The magnitude of the error at the end of the flight is given by,

$$\delta_{error} = v_{p-1}\, dt + m_p\, (1/2)\, a\, dt^2 \tag{9}$$

where p is the total number of sample periods for each flight. Only for the special case where the fielder happens to stop during the flight of the ball at the exact point where the ball will land will $\delta_{error} = 0$.

Using simulations with ball trajectories of varying projection angles (Figure 3), d_n approaches zero for both cases (Figure 7(top)). For the ball with the 45^o projection angle the fielder must run as fast as he can to successfully intercept the ball (Figure 7, middle). For the ball with the 64^o projection angle the fielder accelerates at his maximum rate and then adjusts his velocity sooner than the fielder using the distance to ball strategy (Figure 4(middle)). The fielder using constant acceleration strategy for the 64^o projected ball runs more erratically than the fielder using the distance to ball strategy and appears to more closely match the human results [3]. As for the distance to ball strategy, their point is justified for the 64^o projected ball in that the human fielder does not know where to go to successfully intercept the ball. Otherwise he would run in order to reach the landing point in the shortest time and stop at that point before the ball landed.

Observe in Figure 7(bottom) that the value of $d^2(\tan\alpha_n)/dt^2$ for both the 45^o and 64^o cases stay closer to zero longer than the values recorded using the distance to ball strategy in Section 3.2 (Figure 4(bottom)). Again we observe deviations towards the end of each flight with the drop in $d^2(\tan\alpha_n)/dt^2$ for the 45^o flight indicating the ball drops in front of the fielder and the sporadic values of $d^2(\tan\alpha_n)/dt^2$ for the 64^oflight indicate the ball has passed over the simulated fielder's head at the end of the flight. However, the magnitude of the errors at the ends of both flights are negligible as shown in again in Figure 7(top).

Figure 8 shows the values of the gaze angle, α_n, for each of the four trajectories of varying length. The gaze angle for the ball landing the nearest (-2.9m) to the fielder's initial position approaches 45^o which is to be expected for a parabolic flight assuming the fielder's eyes and ball's projection point are at the same height. This indicates zero error between the ball and the fielder at the time the ball landed. The final gaze angles for the balls landing further away fall short of 45^o which is an indication of the amount of error, δ_{error}, at the time the balls land. This is to be expected since the farther the distance the simulated fielder has to cover the faster he has to run and, by Equation 9, the more error will be induced at the final positions. The error is negligible however compared to the initial distance between the fielder and the ball as can be seen again from the distance to ball plots in Figure 7.

The constant acceleration strategy proved to be successful in the simulations and much more desirable than the distance to ball strategy because the motion control is purely image-based. Therefore, the constant acceleration strategy was implemented with the RWI robot to test the feasibility of McLeod's and Dienes'

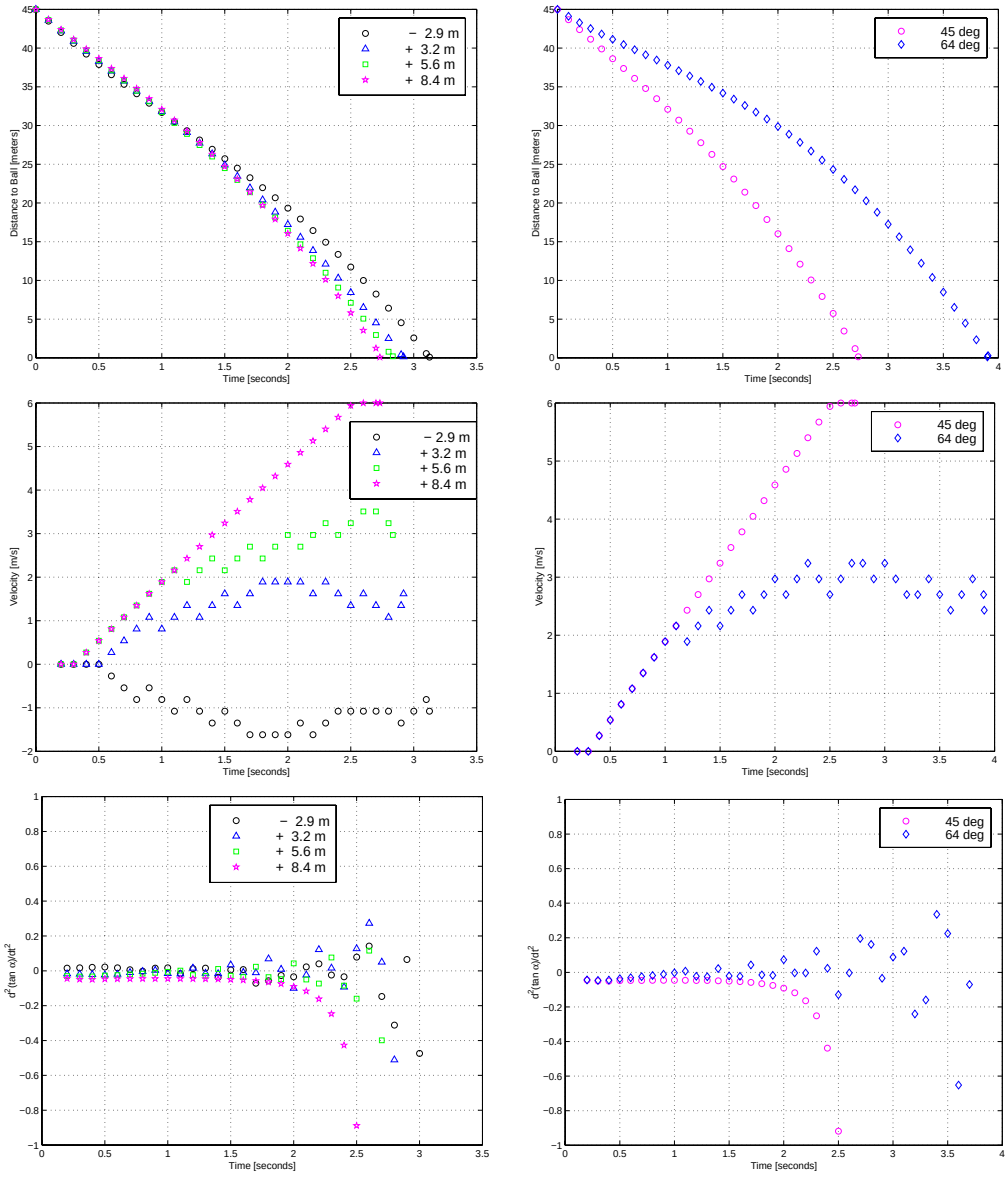

Simulation 1 Simulation 2

Figure 7: Simulation results for constant acceleration strategy (column 1: simulation 1, column 2: simulation 2). Row 1: Distance between the fielder and ball vs. time, Row 2: Fielder velocity vs. time, and Row 3: $d^2(\tan\alpha_n)/dt^2$ vs. time.

model.

4 Robot Fielder Results

As described in Section 2 image based tracking of the ball was achieved by using a white ball against a dark backdrop and using a threshold value to determine the centroid of the ball. The RWI robot was initially placed 3m in front of the projection point of the ball with two video cameras recording the motion of the ball and robot. One video camera tape was used to determine the approximate initial projection angle of the ball while the other recorded both the ball and the robot motion together. The ball was hand-tossed by a human with varying projection angles and velocities. The objective of the robot was to move in order that the onboard CCD camera tracking the ball would make contact with the ball at the end of the flight. For the ideal case the ball would completely fill the image at the time of interception. Twenty-four trials were

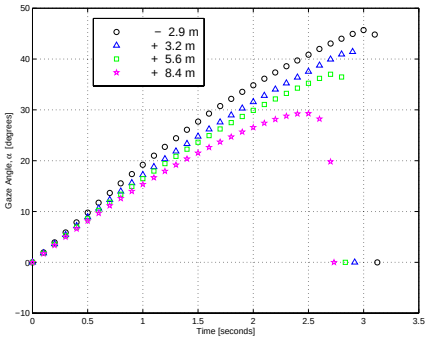

Figure 8: α_n vs. Time

recorded in all with the results of four presented here. For all trials the acceleration of the robot was set to 1200 mm/s^2 and with the parameters $d^2(\tan\alpha_n)/dt^2$ and commanded robot velocity recorded at each sample time (dt = 100ms).

Figure 9 represents the data collected from Trials 4, 9, 14, and 20. The values of the motion parameter $d^2(\tan\alpha_n)/dt^2$ and the corresponding commanded velocity at each point are shown. The initial projection angles determined from analysis of the videotape for Trials 4, 9, 14, and 20 are 55^o, 36^o, 48^o, and 48^o respectively. Also determined from analysis of the videotape was the horizontal distance traveled by each ball between the projection point and the CCD camera's initial position. These distances were approximately 300mm, 450mm, 250mm, and 100mm respectively.

As can be seen from the plots of $d^2(\tan\alpha_n)/dt^2$ (Figure 9, column 1), the values varied in magnitude during the flights much more than the simulated results in Figures 7 and 7 however, the patterns are similar. For each of the robot's results in Trials 4, 9, and 14 the ball dropped in front of the camera towards the end of the flight causing the value of $d^2(\tan\alpha_n)/dt^2$ to decrease. This corresponds to the simulated results for the constant acceleration strategy where the ball lands in front of the fielder at the end of the flight (i.e. +8.4m flight in Figure 7 and 45^o flight in Figure 7) and the value of $d^2(\tan\alpha_n)/dt^2$ decreases rapidly. In Trial 20 the robot successfully intercepts the ball by making contact with the CCD camera which is indicated by the nearly zero final value of $d^2(\tan\alpha_n)/dt^2$.

In Figures 9 (column 2) the commanded velocities for the RWI robot are shown for all 4 trials. By using Equation 7 the velocity was either increased or decreased at each sample time by a factor of the robot's acceleration, a, based on the sign of $d^2(\tan\alpha_n)/dt^2$.

One of the most difficult problems with the trials was the limitation of the lab environment. The human fielder results were for trials where the fielder started much farther from the projection point (45m) and the flight times were much greater than could be achieved in the lab. The ball trajectories were limited by a 3.5m high ceiling where the robot camera was 1.5m off the floor. Additionally the effect of the delay between commanded and actual robot velocities was magnified due to the shortened flight times. For flight times of less than 1 second, the robot had limited ability to react. Optimally the trials would be run where trajectories on the scale of human fielders could be achieved while still tracking the ball. The trial's results however did show matching behavior with the simulated results presented here and with McLeod's and Dienes' results.

5 Conclusions

The goal of this paper was to demonstrate that simple human vision-based approaches to visual-servoing do exist and can be easily implemented. For many visual-servoing tasks dynamic performance is hindered due to the need for geometrical and dynamic modeling. A successful robot motion control strategy was developed for the special case of intercepting balls with projectile motion. This strategy is based on a successful human vision-based strategy which provides a much simpler image-based approach to accomplish the task. The simulated and real-world experimental results presented in this paper have shown the feasibility of this strategy. A mobile robot using this approach can successfully intercept balls with projectile motion and may help provide a basis for the development of human vision-based approaches to visual-servoing in the future.

References

[1] R.L. Andersson. *A Robot Ping-Pong Player.* MIT Press, 1998.

[2] Peter Corke. *Visual Control of Robots.* Research Studies Press, 1996.

[3] Peter McLeod and Zoltan Dienes. *How fielders intercept the ball before it hits the ground.* PhD thesis, Oxford and Sussex University, 1998.

[4] W.H. Press, S.A. Teukolsky, W.T. Vetterling, and B.P. Flannery. *Numerical Recipes in C.* Cambridge University Press, 1988.

[5] Emanuele Trucco and Alessandro Verri. *Introductory Techniques for 3-D Computer Vision.* Prentice-Hall, Inc., 1998.

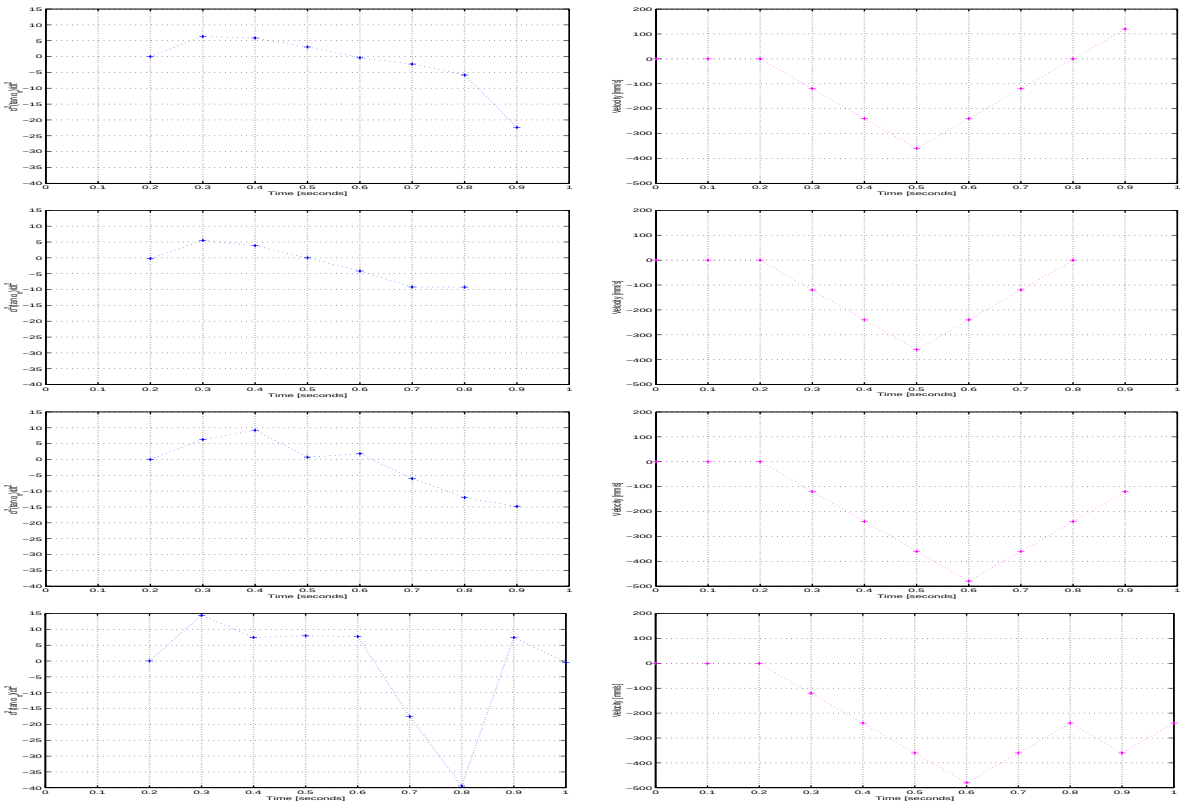

Figure 9: The left hand side shows $d^2(\tan\alpha_n)/dt^2$ vs. Time, the right hand side plots Fielder Velocity vs. Time. Each row shows a different trial (from top to bottom): Trial 4, Trial 9, Trial 14, Trial 20.